Transformation Optics Using Graphene

Ashkan Vakil, *et al.*

Science **332**, 1291 (2011);
DOI: 10.1126/science.1202691

that are still awaiting to be fully explored, and the extreme flexibility of TDSLDA. Because of the complexity of the full 3D TDSLDA equations, these phenomena have never been addressed, even at the mean-field level in fermionic superfluids. Within the TDSLDA framework, one can address with high accuracy on a microscopic basis the real-time dynamics of a UFG superfluid and study quantum turbulence at zero temperature, where dissipative processes are inhibited.

References and Notes

1. L. Tisza, *Nature* **141**, 913 (1938).
2. L. Landau, *J. Phys. USSR* **5**, 71 (1941).
3. L. Onsager, *Nuovo Cim.* **6**, 279 (1949).
4. R. P. Feynman, in *Progress in Low Temperature Physics*, vol. 1, C. J. Gorter, Ed. (North-Holland, Amsterdam, 1955), pp. 17–53.
5. V. L. Ginzburg, L. D. Landau, *Zh. Eksp. Teor. Fiz.* **20**, 1064 (1950).
6. A. A. Abrikosov, *Sov. Phys. JETP* **5**, 1174 (1957).
7. E. P. Gross, *Nuovo Cim.* **20**, 454 (1961).
8. L. P. Pitaevskii, *Sov. Phys. JETP* **13**, 451 (1961).
9. W. F. Vinen, R. J. Donnelly, *Phys. Today* **60**, 43 (2007).
10. L. D. Landau, *J. Phys. USSR* **11**, 91 (1947).
11. I. S. Aranson, L. Kramer, *Rev. Mod. Phys.* **74**, 99 (2002), and references therein.
12. A. Bulgac, S. Yoon, *Phys. Rev. Lett.* **102**, 085302 (2009).
13. E. A. Yuzbashyan, O. Tsyplyatyev, B. L. Altshuler, *Phys. Rev. Lett.* **96**, 097005 (2006).
14. S. Giorgini, L. P. Pitaevskii, S. Stringari, *Rev. Mod. Phys.* **80**, 1215 (2008).
15. I. Bloch, J. Dalibard, W. Zwerger, *Rev. Mod. Phys.* **80**, 885 (2008).
16. W. Ketterle, M. W. Zwierlein, "Making, probing and understanding ultracold Fermi gases," in *Ultracold Fermi Gases, Proceedings of the International School of Physics "Enrico Fermi,"* vol. 164, M. Inguscio, W. Ketterle, C. Salomon, Eds. (IOS Press, Amsterdam, 2007).
17. G. A. Baker Jr., *Phys. Rev. C Nucl. Phys.* **60**, 054311 (1999).
18. J. Carlson, S. Y. Chang, V. R. Pandharipande, K. E. Schmidt, *Phys. Rev. Lett.* **91**, 050401 (2003).
19. K. M. O'Hara, S. L. Hemmer, M. E. Gehm, S. R. Granade, J. E. Thomas, *Science* **298**, 2179 (2002); 10.1126/science.1079107.
20. M. W. Zwierlein, J. R. Abo-Shaeer, A. Schirotzek, C. H. Schunck, W. Ketterle, *Nature* **435**, 1047 (2005).
21. R. Sensarma, M. Randeria, T. L. Ho, *Phys. Rev. Lett.* **96**, 090403 (2006).
22. R. M. Dreizler, E. K. U. Gross, *Density Functional Theory: An Approach to the Quantum Many-Body Problem* (Springer, Berlin, 1990).
23. E. Runge, E. K. U. Gross, *Phys. Rev. Lett.* **52**, 997 (1984).
24. A. Bulgac, M. M. Forbes, P. Magierski, http://arxiv.org/abs/1008.3933.
25. A. Bulgac, K. J. Roche, *J. Phys. Conf. Ser.* **125**, 012064 (2008).
26. G. Tonini, F. Werner, Y. Castin, *Eur. Phys. J. D* **39**, 283 (2006).
27. A. Bulgac, *J. Phys. G Nucl. Part. Phys.* **37**, 064006 (2010).
28. N. G. Parker, B. Jackson, A. M. Martin, C. S. Adams, in *Emergent Nonlinear Phenomena in Bose-Einstein Condensates*, P. G. Kevrekidis, D. J. Frantzeskakis, R. Carretero-Gonzales, Eds. (Springer, Berlin, 2008), pp. 173–190.
29. A. Bulgac, Y. Yu, *Phys. Rev. Lett.* **91**, 190404 (2003).
30. N. Nygaard, G. M. Bruun, C. W. Clark, D. L. Feder, *Phys. Rev. Lett.* **90**, 210402 (2003).

Acknowledgments: We thank G. F. Bertsch for discussions. This work was supported by U.S. Department of Energy (DOE) grants DE-FG02-97ER41014, DE-FC02-07ER41457, DE-AC05-76ORL01830; grant no. N N202 128439 from the Polish Ministry of Science; and grants NSF-11075201 and NKBRSF-2011CB921503 from the People's Republic of China. Calculations have been performed on Univ. of Washington (UW) Athena, Hyak UW (NSF Major Research Instrumentation grant PHY-0922770), Franklin (Cray XT4, National Energy Research Scientific Computing Center, DOE grant B-AC02-05CH11231), and JaguarPF (Cray XT5, National Center for Computational Sciences, DOE grant DE-AC05-00OR22725). Movies clips of the simulations are archived at www.phys.washington.edu/groups/qmbnt/UFG/ (see SOM for instructions).

Supporting Online Material

www.sciencemag.org/cgi/content/full/332/6035/1288/DC1
SOM Text
Figs. S1 to S7
Tables S1 to S5
References
Movies S1 to S40 at www.phys.washington.edu/groups/qmbnt/UFG/

21 December 2010; accepted 11 April 2011
10.1126/science.1201968

Transformation Optics Using Graphene

Ashkan Vakil and Nader Engheta*

Metamaterials and transformation optics play substantial roles in various branches of optical science and engineering by providing schemes to tailor electromagnetic fields into desired spatial patterns. We report a theoretical study showing that by designing and manipulating spatially inhomogeneous, nonuniform conductivity patterns across a flake of graphene, one can have this material as a one-atom-thick platform for infrared metamaterials and transformation optical devices. Varying the graphene chemical potential by using static electric field yields a way to tune the graphene conductivity in the terahertz and infrared frequencies. Such degree of freedom provides the prospect of having different "patches" with different conductivities on a single flake of graphene. Numerous photonic functions and metamaterial concepts can be expected to follow from such a platform.

The fields of plasmonics, metal optics, metamaterials, and transformation optics (*1*–*8*) offer a collection of techniques to tame the electromagnetic fields into desired spatial patterns, providing applications in engineering and applied sciences. Owing to their ability to support the surface-plasmon polariton (SPP) surface waves in the infrared and visible regimes, the noble metals, such as silver and gold, have been popular materials for constructing optical metamaterials (*1*). However, the difficulty in controlling and varying permittivity functions of noble metals and the existence of material losses—especially at visible wavelengths—degrade the quality of the plasmon resonance and limit the relative propagation lengths of SPP waves along the interface between such metals and dielectric materials. These drawbacks constrain the functionality of some of metamaterials and transformation optical devices. We show that graphene, which has exciting electronic transport properties (*9*, *10*) suitable for optoelectronic applications (*11*–*16*), may also serve as a platform for metamaterials and transformation optical devices.

Graphene's complex conductivity ($\sigma_g = \sigma_{g,r} + i\sigma_{g,i}$) depends on the radian frequency ω, charged particle scattering rate Γ representing the loss mechanism, temperature T, and chemical potential μ_c. The chemical potential depends on the carrier density and can be controlled by gate voltage, electric field, magnetic field, and/or chemical doping (*17*, *18*). The imaginary part of graphene conductivity can attain negative and positive values in different ranges of frequencies depending on the level of chemical potential (*17*). The complex conductivity of a free-standing isolated graphene at $T = 3$ K, with $\Gamma = 0.43$ meV (*17*)—computed from the Kubo formula, which is in agreement with experimental results (*18*)—shows regions of frequencies and chemical potentials for which $\sigma_{g,i} < 0$, whereas for other regions $\sigma_{g,i} > 0$ (Fig. 1, A and B). When $\sigma_{g,i} > 0$, a graphene layer effectively behaves as a very thin "metal" layer (*19*) capable of supporting a transverse-magnetic (TM) electromagnetic SPP surface wave (*20*–*23*). The dispersion relation of this TM SPP surface wave is expressed as $\beta^2 = k_0^2[1 - (2/\eta_0\sigma_g)^2]$, where β and k_0 are, respectively, the wave numbers of the guided mode and the free space, and η_0 is the intrinsic impedance of free space (*19*–*22*). However, when $\sigma_{g,i} < 0$, TM SPP guided surface wave is no longer supported by the graphene. Instead, a weakly guided transverse-electric (TE) electromagnetic SSP surface wave might be present (*19*–*21*). There are at least two major advantages for a graphene layer as compared with the noble metal surfaces: (i) As far as the SPP characteristics are concerned, in the mid infrared (IR) wavelengths the combination of two features of SPP—the propagation length, defined as 1/Im (β), and the mode lateral extent, proportional to approximately 1/Re(β)—for graphene can be more favorable than for silver or gold (*19*); the real part of wave number β for the TM SPP wave along the graphene is much larger than the wave number of free space, $k_0 \equiv \omega(\mu_0\varepsilon_0)^{1/2}$ (fig. S1A) (*19*). As a result, such a SPP surface wave is tightly confined to the graphene layer, with guided wavelength (λ_{SPP}) much smaller than free space wavelength λ_0 ($\lambda_{SPP} << \lambda_0$), whereas its imaginary part of wavenumber is small (*22*, *24*). (ii) The most important advantage of graphene over thin metal layers and metal interfaces is the capability to dynamically tune the conductivity of graphene by means

Department of Electrical and Systems Engineering, University of Pennsylvania, Philadelphia, PA 19104, USA.

*To whom correspondence should be addressed. E-mail: engheta@ee.upenn.edu

of chemical doping or gate voltage—E_{bias} in real time, locally and inhomogeneously. By using different values of E_{bias} at different locations across the single graphene layer, we can create certain desired conductivity patterns.

We present several scenarios in which the proper choice of conductivity spatial patterns across the graphene provides exciting possibilities for tailoring, manipulating, and scattering IR SPP wave signals across the graphene. To start, consider a SPP mode at 30 THz guided by a uniformly biased graphene layer (fig. S2) (*19*). The TM SPP–guided wavelength λ_{SPP} for this free-standing graphene in air at $T = 3$ K with $\Gamma = 0.43$ meV and $\mu_c = 0.15$ eV is $\lambda_0/69.34 = 144.22$ nm, with $\mathrm{Re}(\beta) = 69.34k_0$ and $\mathrm{Im}(\beta) = 0.71k_0$. This highly compressed mode offers an effective SPP index ($n_{SPP} \equiv \beta_{SPP}/k_0$) of 69.34 and has a relatively large propagation length of $15.6\lambda_{SPP} = 0.225\lambda_0 = 2.25$ μm. We can engineer the SPP surface wave to reflect and refract on this sheet of graphene (Fig. 2) by varying the electric field bias spatially. To achieve spatially varying static electric field bias, one may consider three possible methods: (i) a split gate structure to apply different bias voltages to different gates (Fig. 2). The potentials V_{b1} and V_{b2}, applied to two gate electrodes, are chosen to provide different chemical potential values, such as $\mu_{c1} = 0.15$ eV and $\mu_{c2} = 0.065$ eV, in the two halves of graphene. For the sake of clarity, in Fig. 2 the "gate electrodes" are symbolically shown above the graphene at a small distance. However, the gates may be located on the substrate beneath the graphene. (ii) An uneven ground plane (Fig. 3, A and B, and figs. S7 and S8). By designing the specific profile of the ground plane underneath the dielectric spacer holding the graphene, one can achieve nonuniform static biasing electric field under the graphene, resulting in different conductivity values at different segments of graphene (*19*). (iii) Inhomogeneous permittivity distribution near the top surface of the spacer holding a sheet of graphene (fig. S9) (*19*). Inhomogeneous distribution of permittivity generates a nonuniform static electric field under the graphene, creating inhomogeneous chemical potential and in turn inhomogeneous conductivity across the graphene (*19*).

In Fig. 2, the conductivity values of the two segments calculated from the Kubo formula with $T = 3$ K and $\Gamma = 0.43$ meV are, respectively, $\sigma_{g1} = 0.0009 + i0.0765$ mS and $\sigma_{g2} = 0.0039 - i0.0324$ mS. The "farther" half section with $\sigma_{g1,i} > 0$ supports a TM SPP, whereas the "closer" half with $\sigma_{g1,i} < 0$ does not. If a TM SPP is launched in the farther-half section toward the junction of two sections, it reflects back at that boundary line. Then, the incident and reflected SPP waves add up to form an oblique standing wave. The reflection of SPP at this line resembles the Fresnel reflection of a plane wave from a planar interface between two media. Here, however, such reflection occurs across a one-atom-thick platform, with a favorably little radiation loss owing to high confinement of SPP to the graphene. This case might also be analogous to the Fresnel reflection from a planar interface between a medium that supports propagating waves (for example, a medium with a real refractive index, such as a dielectric) and another medium that does not support propagating waves (for example, a medium with no real index, such as a noble metal). Accordingly, on the graphene the Fresnel reflection of SPP results in a near complete reflection. The simulation results reveal an effective reflection at the boundary line between the two segments. In Fig. 2, a guided IR edge wave along the boundary line between the two sections can be observed (*19*). This phenomenon might be related to the electronic behavior near the p-n junction formed on the graphene (*13*, *14*, *25*).

On the basis of the reflection mechanism mentioned above, we propose a setting analogous to a conventional three-dimensional (3D) metal-insulator-metal (MIM) waveguide, but here on a one-atom-thick platform (Fig. 3A). This 2D waveguide variant consists of three distinct regions on the graphene: two side regions with chemical potential μ_{c2} resulting in conductivity $\sigma_{g2} = 0.0039 - i0.0324$ mS where $\sigma_{g2,i} < 0$, and a middle "ribbon-like" section, with chemical potential μ_{c1} yielding conductivity $\sigma_{g1} = 0.0009 + i0.0765$ mS where $\sigma_{g1,i} > 0$. An uneven ground plane, for example, can be used to achieve these two different chemical potentials (*19*). However, because the SPP is highly confined to the graphene, in all our numerical simulations the graphene is assumed to be free standing in vacuum (*26*). A guided SPP wave is bounded by the two boundary lines between the graphene sections with different conductivities, as shown in Fig. 3A. Moreover, an IR splitter, based on the waveguide concept, might be envisioned. This can be achieved by proper design of conductivity patterns on the graphene, generated, for example, by use of uneven ground plane or other techniques (*19*) to create required spatial distribution

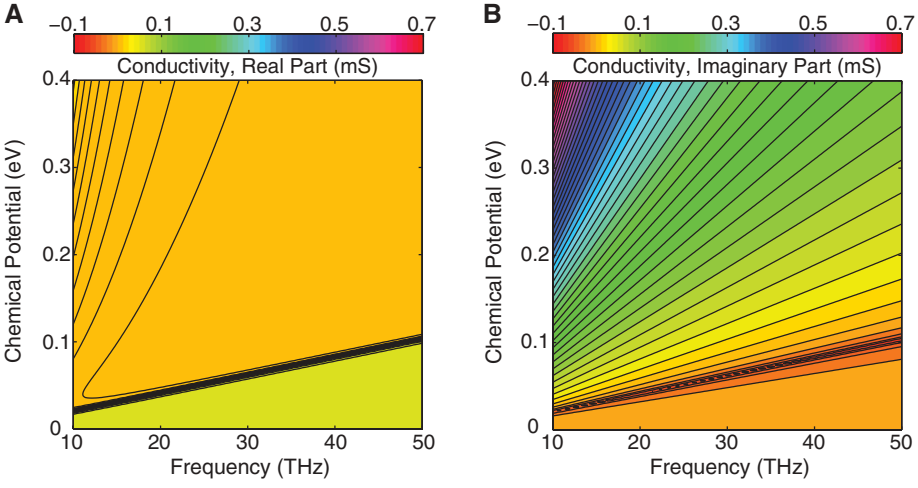

Fig. 1. (**A**) Real part and (**B**) imaginary part of the conductivity as a function of the chemical potential and frequency ($T = 3$ K, $\Gamma = 0.43$ meV), following the Kubo formula (*17*).

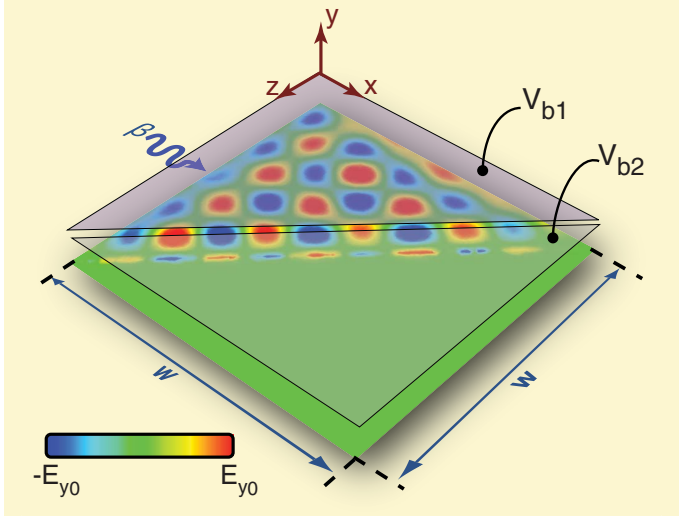

Fig. 2. Simulation results showing snap shot in time of y component of the electric field, E_y for the near total reflection of a TM electromagnetic SPP wave on a free-standing graphene ($w = 800$ nm, $T = 3$ K, $\Gamma = 0.43$ meV, $\mu_c = 0.15$ eV). The V_{b1} and V_{b2} are chosen so that the two halves of graphene acquire complex conductivity values $\sigma_{g1} = 0.0009 + i0.0765$ mS and $\sigma_{g2} = 0.0039 - i0.0324$ mS.

of the bias electric field (Fig. 3B). The mechanism for guiding IR signals across the graphene offers the possibility of contriving miniaturized, one-atom-thick photonic circuitry for information processing at the nanoscale (*19*, *27*).

On the basis of the proposed concepts, one can also envisage 2D IR metamaterials and transformation optical devices on a single layer of carbon atoms. Figure 4A shows numerical simulation of SPP propagation along a free-standing layer of graphene, within which an array of 2D circular "patches" is created. These patches are biased at voltage V_{b2} ($\sigma_{g2} = 0.0039 - i0.0324$ mS, where $\sigma_{g2,i} < 0$), whereas the rest of graphene is biased at V_{b1} ($\sigma_{g1} = 0.0009 + i0.0765$ mS, where $\sigma_{g1,i} > 0$). Each circular patch acts as a scatterer for the SPP surface wave, behaving as a single-atom-layered "flatland inclusion." The collection of these "inclusions" can result in a 2D bulk flat metamaterial. Our numerical simulations suggest that such geometry, if designed properly, can act as a 2D version of metamaterials formed by collection of subwavelength metallic nanoparticles that may, under certain conditions, exhibit backward wave propagation effect (*28*). Furthermore, a "flat" version of a Luneburg lens, which is an example of transformation optical devices (*29*, *30*), is presented in Fig. 4B. Such graphene-based Luneburg lens can be designed by creating several concentric rings with specific conductivity values. With a special configuration of bias arrangement, we can create, approximately, a graded conductivity pattern that provides the required effective SPP-graded index for operation of the Luneburg lens. To find the corresponding conductivities for these concentric rings (for a Luneburg lens with diameter D), we used the discretized approximate expression $\sigma_{i,n} = \sigma_{i,out}\{2 - [(r_n + r_{n-1})/D]^2\}^{-1/2}$ (*19*), where $\sigma_{i,n}$ and r_n denote, respectively, the imaginary part of conductivity and radius of the n^{th} section, and $\sigma_{i,out}$ is the imaginary part of conductivity of the background graphene. Our simulation results (Fig. 4B) reveal that the SPP generated from a "point-like" source is evolved into an approximately one-atom-thick "collimated beam" of SPP on the graphene, as a conventional 3D Luneburg lens collimates wavefronts generated from a point source into a 3D beam. The diameter of the "flat" Luneburg lens is about 1.5 μm, which is $0.15\lambda_0$—a notably subwavelength size. This example suggests that various subwavelength IR devices (such as convex lenses and concave lenses) can be designed on the graphene, providing a versatile platform for nanoscale Fourier optics and other photonic signal–processing methods.

Our theoretical study of IR wave interaction with graphene suggests that the graphene can be a low-loss one-atom-thick platform for flatland IR metamaterials and transformative optics. The inhomogeneous, nonuniform patterning of conductivity may be achieved by various techniques, for example, by creating uneven ground plane, fabricating inhomogeneous permittivity of spacer dielectric, and applying gate electric or magnetic field.

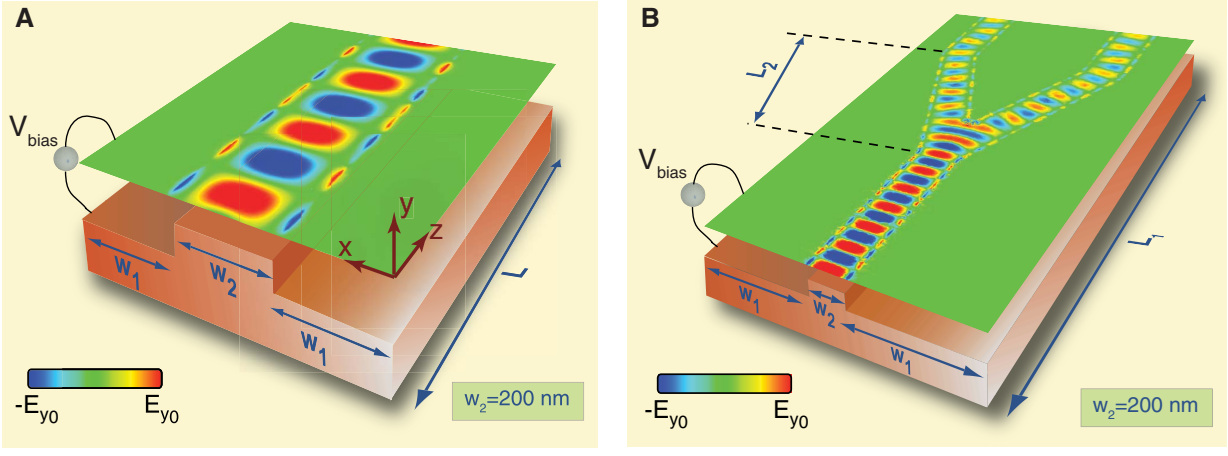

Fig. 3. (**A**) Simulation results of E_y (snap shot in time) for an IR-guided wave at f = 30 THz along the ribbon-like section of graphene with the chemical potential μ_{c1} (L = 560 nm, $w = w_1 + w_2 + w_3$ = 200 + 200 + 200 nm). (**B**) Similar to (A), but here the ribbon-like section splits into two paths (L_1 = 1077 nm, L_2 = 560 nm, $w = w_1 + w_2 + w_3$ = 600 + 200 + 600 nm) (*26*). Different scale bars in each panel. The graphene conductivity parameters are similar to those in Fig. 2.

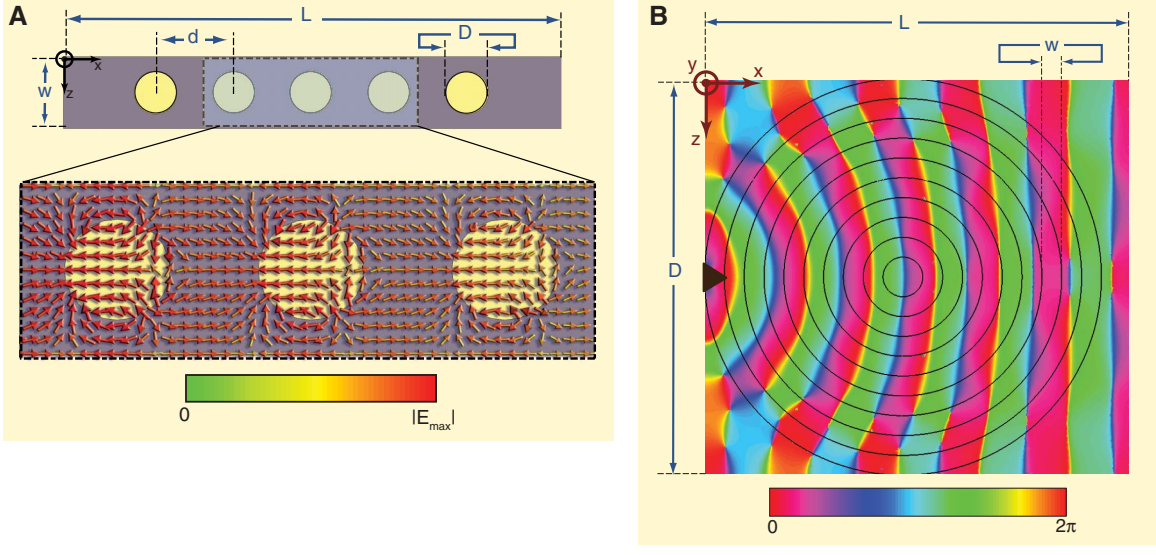

Fig. 4. (**A**) Flatland metamaterial: the snap shot in time of the electric field vectors for the TM SPP along a single sheet of graphene at f = 30 THz, shown on the graphene plane. Only one row of the 2D periodic array is shown (D = 30 nm, $d = w$ = 55 nm, L = 370 nm). (**B**) One-atom-thick Luneburg lens: Simulation results showing the phase of E_y of the SPP at f = 30 THz along the graphene (D = 1.5 μm, w = 75 nm, L = 1.6 μm).

References and Notes

1. W. Cai, V. Shalaev, *Optical Metamaterials: Fundamentals and Applications* (Springer, New York, 2010).
2. D. R. Smith, J. B. Pendry, M. C. K. Wiltshire, *Science* **305**, 788 (2004).
3. N. Engheta, R. W. Ziolkowski, *Metamaterials, Physics and Engineering Explorations* (IEEE-Wiley, New York, 2006).
4. G. V. Eleftheriades, K. G. Balmain, *Negative-Refraction Metamaterials* (IEEE, New York, 2005).
5. J. B. Pendry, D. Schurig, D. R. Smith, *Science* **312**, 1780 (2006).
6. D. Schurig *et al.*, *Science* **314**, 977 (2006).
7. U. Leonhardt, *Science* **312**, 1777 (2006).
8. S. Maier, *Plasmonics: Fundamentals and Applications* (Springer, New York, 2007).
9. K. S. Novoselov *et al.*, *Nature* **438**, 197 (2005).
10. A. K. Geim, K. S. Novoselov, *Nat. Mater.* **6**, 183 (2007).
11. D. R. Anderson, *J. Opt. Soc. Am. B* **27**, 818 (2010).
12. F. Rana, *IEEE Trans. NanoTechnol.* **7**, 91 (2008).
13. E. G. Mishchenko, A. V. Shytov, P. G. Silvestrov, *Phys. Rev. Lett.* **104**, 156806 (2010).
14. V. V. Cheianov, V. Fal'ko, B. L. Altshuler, *Science* **315**, 1252 (2007).
15. P. R. West *et al.*, *Laser Photon. Rev.* **4**, 795 (2010).
16. N. Papasimakis *et al.*, *Opt. Express* **18**, 8353 (2010).
17. V. P. Gusynin, S. G. Sharapov, J. P. Carbotte, *J. Phys. Condens. Matter* **19**, 026222 (2007).
18. Z. Q. Li *et al.*, *Nat. Phys.* **4**, 532 (2008).
19. Materials and methods are available as supporting material on *Science* Online.
20. G. W. Hanson, *J. Appl. Phys.* **103**, 064302 (2008).
21. S. A. Mikhailov, K. Ziegler, *Phys. Rev. Lett.* **99**, 016803 (2007).
22. M. Jablan, H. Buljan, M. Soljacic, *Phys. Rev. B* **80**, 245435 (2009).
23. E. H. Hwang, S. D. Sarma, *Phys. Rev. B* **75**, 205418 (2007).
24. For example, for a layer of graphene free standing in air at $T = 3$ K with $\Gamma = 0.43$ meV and $\mu_c = 0.15$ eV at frequency 30 THz, $\mathrm{Re}(\beta) = 69.34k_0$ and $\mathrm{Im}(\beta) = 0.71k_0$. The corresponding numbers for the SPP at the air-silver interface in the mid IR wavelengths are approximately $\mathrm{Re}(\beta) \approx k_0$ and $\mathrm{Im}(\beta) < 10^{-4}k_0$, resulting in a very weakly confined SPP.
25. R. Dehbashi, D. Fathi, S. Mohajerzadeh, B. Forouzandeh, *IEEE J. Sel. Top. Quantum Electron.* **16**, 394 (2010).
26. The formation of such highly confined SPP is not due to direct interaction of light with the ground plane because obviously the confined SPP still exists for a free-standing graphene. The SPP wave is so highly confined that its field does not even "touch" the ground plane underneath. Therefore, without loss of generality, in all of our numerical studies the simulations are performed for the free-standing graphene in vacuum and with no ground plane present.
27. N. Engheta, *Science* **317**, 1698 (2007).
28. A. Alu, N. Engheta, *Phys. Rev. B* **75**, 024304 (2007).
29. T. Zentgraf, Y. Liu, M. H. Mikkelsen, J. Valentine, X. Zhang, *Nat. Nanotechnol.* **6**, 151 (2011).
30. P. A. Huidobro, M. L. Nesterov, L. Martín-Moreno, F. J. García-Vidal, *Nano Lett.* **10**, 1985 (2010).

Acknowledgments: This work is supported in part by the U.S. Air Force Office of Scientific Research (AFOSR) grants FA9550-08-1-0220 and FA9550-10-1-0408. Authors have no conflict of interest. A provisional patent application on the ideas presented in this manuscript has been filed by the University of Pennsylvania.

Supporting Online Material

www.sciencemag.org/cgi/content/full/332/6035/1291/DC1
Materials and Methods
SOM Text
Figs. S1 to S9
References

10 January 2011; accepted 11 April 2011
10.1126/science.1202691

Wafer-Scale Graphene Integrated Circuit

Yu-Ming Lin,* Alberto Valdes-Garcia, Shu-Jen Han, Damon B. Farmer, Inanc Meric,† Yanning Sun, Yanqing Wu, Christos Dimitrakopoulos, Alfred Grill, Phaedon Avouris,* Keith A. Jenkins

A wafer-scale graphene circuit was demonstrated in which all circuit components, including graphene field-effect transistor and inductors, were monolithically integrated on a single silicon carbide wafer. The integrated circuit operates as a broadband radio-frequency mixer at frequencies up to 10 gigahertz. These graphene circuits exhibit outstanding thermal stability with little reduction in performance (less than 1 decibel) between 300 and 400 kelvin. These results open up possibilities of achieving practical graphene technology with more complex functionality and performance.

Graphene, a layer of carbon atoms arranged in a hexagonal lattice, is a promising candidate for future high-speed electronics and radio-frequency (RF) applications (*1*–*4*) because of its high carrier mobility and saturation velocity (*5*). The planar structure and the feasibility of large-area graphene synthesis facilitate the adoption of top-down device fabrication techniques. Graphene transistors with intrinsic cut-off frequencies beyond 100 GHz have been recently achieved by several groups using graphene films synthesized by various methods, including epitaxial growth on SiC (*6*, *7*), chemical vapor deposition (CVD) on Cu (*8*), and mechanical exfoliation (*9*, *10*). The monolithic integration of transistors with interconnects and other components is an essential requirement for any semiconductor material to achieve a widespread technological impact. Previous attempts to make circuits based on graphene have used an indi-

IBM Thomas J. Watson Research Center, Yorktown Heights, NY 10598, USA.

*To whom correspondence should be addressed. E-mail: yming@us.ibm.com (Y.-M.L.); avouris@us.ibm.com (P.A.)
†Present address: Columbia University, New York, NY 10027, USA.

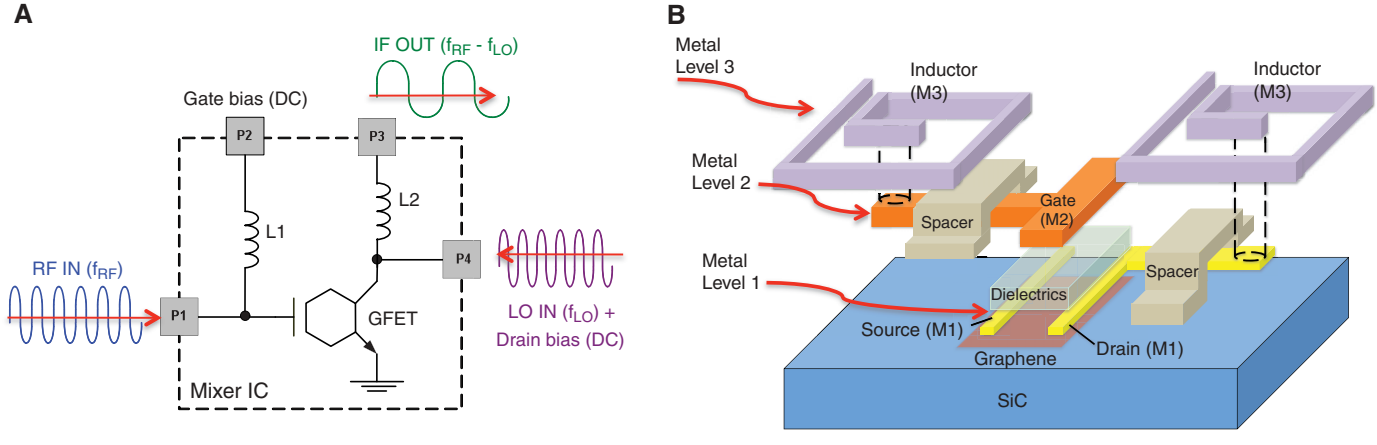

Fig. 1. (**A**) Circuit diagram of a four-port graphene RF frequency mixer. The scope of the graphene IC is confined by the dashed box. The hexagonal shape represents a graphene FET. (**B**) Schematic exploded illustration of a graphene mixer circuit. The critical design aspects include a top-gated graphene transistor and two inductors connected to the gate and the drain of the GFET. Three distinct metals layers of the graphene IC are represented by M1, M2, and M3. A layer of 120-nm-thick SiO_2 is used as the isolation spacer to electrically separate the inductors (M3) from the underlying interconnects (M1 and M2).